

# Numerical modelling of inhibited electrical discharges in air

Anders Larsson<sup>†</sup>, Anne Bondiou-Clergerie<sup>‡</sup> and Ivo Gallimberti<sup>§</sup>

<sup>†</sup> Institute of High Voltage Research, Uppsala University, Husbyborg, S-752 28 Uppsala, Sweden

<sup>‡</sup> Office National d'Etudes et Recherches Aerospatiales, 29 av. de la Division Leclerc, Chatillon sous Bagneux, France

<sup>§</sup> Department of Electrical Engineering, University of Padua, Italy

Received 3 December 1997, in final form 30 March 1998

**Abstract.** The *inhibited discharge* is a discharge in which the input of energy into the discharge channel is limited by the presence of a large series resistance in the external circuit supplying the discharge current. One situation in which such a discharge occurs is in outdoor high-voltage insulation systems when the system is subjected to rain. The inhibiting resistance is caused by layers or runnels of water on the insulator's surface. This paper concentrates upon the numerical modelling of the inhibited discharge. The core of the modelling is the interaction between the discharge itself and the external circuit which supplies the discharge current. Physical models of the corona streamer development, the propagation of the streamer–leader system and the final jump were used for the calculation of the discharge current. The calculations show that propagation of the streamer is not influenced by a large series resistance, whereas the propagation of the streamer–leader system and the final jump may be significantly inhibited.

## 1. Introduction

Safe transmission and distribution of electrical power is partly determined by the reliability of the electrical insulation system of the power lines and substations. By applying a detailed knowledge of the fundamental discharge processes that occur prior to the disruptive discharge, one can predict the behaviour of outdoor high-voltage insulator systems in operation under all possible atmospheric conditions. One of these discharge processes is the *inhibited discharge*, in which the input of energy into the ionized channels is limited by a large series resistance in the external circuit (Larsson 1997). In reality, such discharges occur under the operation of outdoor high-voltage insulators subjected to rain, for which the inhibiting resistance is from layers of water or runnels on the surface of the insulators. For a concise review of previous studies of inhibited discharges, see Larsson (1998).

The inhibited discharge has recently been studied experimentally (Larsson 1998) for a 1 m rod-to-plane gap subjected to switching impulses: the main results were that the disruptive discharge voltage increases with the series resistance and that both the time lapse between the application of the voltage and the initiation of the final jump and the duration of the final jump are substantially prolonged. All the experimental results used in this paper originate from Larsson (1998) unless otherwise stated.

The objective of this work is to present numerical models of the inhibited discharge in order to provide a

physical interpretation of the experimental results presented by Larsson (1998). The basic feature of the inhibited discharge to be modelled is the interaction between the discharge itself and the external circuit that supplies the discharge current; this is treated in section 2. The subsequent phases of the spark discharge development (Gallimberti 1979) which can be inhibited by a large series resistance are:

- (i) the formation of the streamer corona,
- (ii) the propagation of the streamer–leader system and
- (iii) the final jump.

Models of each of these phases are presented and discussed in sections 3, 4 and 5, respectively. For the formation of the streamer corona and the propagation of streamer–leader system existing models have been used (Gallimberti 1972, Goelian *et al* 1997). A model of the final jump is developed in this paper.

## 2. The inhibited discharge circuit

The reference experimental set-up is given in figure 1(a), whereas figure 1(b) shows a simplified equivalent circuit. In these figures,  $U_0 = U_0(t)$  is the applied voltage and  $U = U(t)$  is the gap voltage;  $R$  is the series resistance and  $C_R$  is its stray capacitance,  $C_g$  is the gap capacitance and  $I_d$  is the discharge current. The presence of a large series resistance in the discharge circuit means that the gap voltage is not equal to the applied voltage because

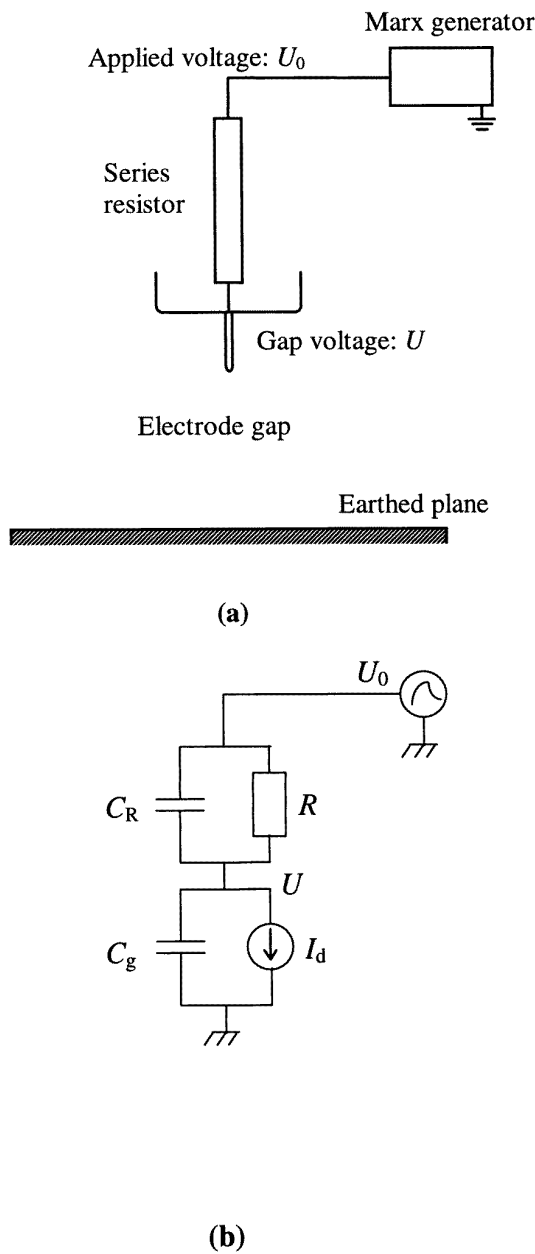


**Figure 1.** (a) The reference experimental set-up for the study of inhibited discharges and (b) the equivalent circuit.

of the following two effects (Larsson and Scuka 1997): firstly, the voltage division caused by the series resistance and its stray capacitance in series with the gap capacitance and, secondly, the voltage drop caused by the discharge current. The equivalent circuit of figure 1(b) can be easily modelled, because the parameters  $R$ ,  $C_R$  and  $C_g$  can be determined by measurement or calculation. The only external parameter that remains to be modelled is the discharge current  $I_d$  which depends nonlinearly on the gap voltage. The differential equation for this circuit is

$$C_R \frac{d(U_0 - U)}{dt} + \frac{U_0 - U}{R} = C_g \frac{dU}{dt} + I_d$$

$$I_d = f(U) \tag{1}$$

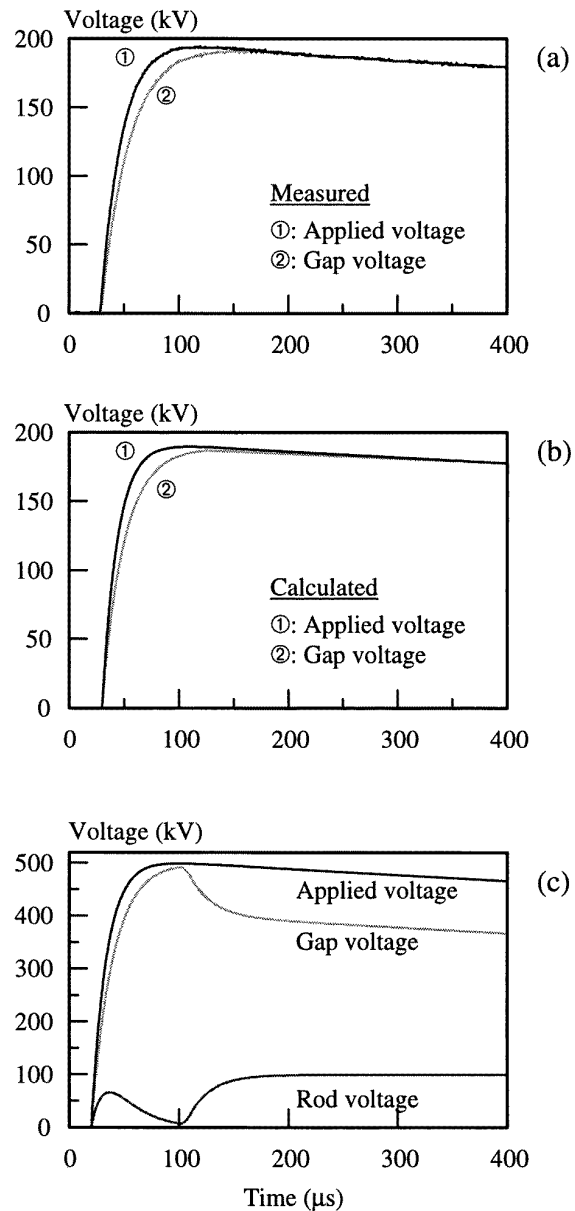


**Figure 2.** (a) The measured and (b) calculated voltage for a typical corona-free case. (c) Results of a calculation with a predefined step current of 0.1 A injected at 100 μs. These results show the voltage division, namely the difference between the applied voltage and the gap voltage, caused by the circuit components.

which has to be solved numerically. A simple Euler forwards time-stepping method has been used without encountering numerical problems. The stray capacitances of the gap and the resistor have been estimated by means of an electrostatic field calculation (Ace 1996); for the reference experimental set-up, the values were  $C_g = 6$  pF and  $C_R = 15$  pF, with  $R = 1$  MΩ.

A measurement of the gap voltage in the absence of a discharge current, that is, a corona-free measurement, is presented in figure 2(a) and is compared with a numerical solution of (1) with  $I_d = 0$  (figure 2(b)). These results

show the voltage division caused by the circuit components. The good agreement between the measurements and the simulation validates the equivalent circuit parameters.

In order to illustrate the effect of the discharge current on the gap voltage, a predefined current has been used in the simulation (a step current of 0.1 A with a rise time of 10 ns applied at 100  $\mu$ s). Figure 2(c) shows the simulated results, with a lowering of the gap voltage corresponding to the flow of the discharge current.

We developed a more detailed model of the series resistor in which the resistor was represented by distributed resistance, capacitance and inductance and the results were compared with those from the simple circuit model of figure 1(b) (Larsson 1997). This comparison revealed the more detailed model gave a slightly faster reduction in the gap voltage than did the simple model, but the difference was found to be negligible for the present study.

### 3. The streamer corona phase

#### 3.1. The streamer inception model

The fundamental process in electrical discharges is the multiplication of free electrons (electron avalanches) caused by direct ionization driven by the external electric field (Meek and Craggs 1978, Gallimberti 1979). If the external field is sufficiently high, the space charge in the avalanche tip creates an electrical field that significantly adds to the external electrical field distribution in the vicinity of the tip. If new avalanches can be initiated close to the first one, the avalanche has grown to the critical size when the avalanche-to-streamer transition takes place (streamer inception). At least one free, seeding electron is needed to initiate the avalanche and the time lag between attainment of the electrical field necessary for formation of the critical avalanche and its actual occurrence is called the statistical time lag.

The threshold voltage for inception of a streamer corona was calculated by integrating the effective ionization coefficient along the most stressed field line; that is, by solving the equation for the critical avalanche presented by Gallimberti (1979). The value calculated is the minimum inception voltage. The value of the actual streamer inception voltage may be considerably higher due to there being a deficiency of seeding electrons. No model for the production of seeding electrons, namely, a model to calculate the statistical time lag, has been implemented. The influence of this time lag was investigated by systematically increasing the actual inception voltage in the model outlined below.

#### 3.2. The streamer propagation model

Once it has been initiated, the streamer propagation can be described in the following manner (Gallimberti 1972). In front of the streamer, the external field is added to the space-charge field associated with the charge in the streamer's head. New avalanches are launched in the high-field region near the streamer's tip where the electrical field is so strong that ionization exceeds attachment (the active

region). These new avalanches are directed towards the streamer's head and the positive space charge in their wake will form the new streamer tip. If the space-charge field from the new streamer tip, together with the external field, is sufficiently high to produce new avalanches, the streamer will propagate. Otherwise it will stop.

The streamer propagation was calculated using Gallimberti's model (Gallimberti 1972), in which he replaces the multiple avalanches in the active region by one equivalent avalanche that produces the same amount of space charge as the multiple ones. The starting point of the equivalent avalanche is determined by the energy balance equation

$$W_g + \Delta W_{pot} = W_l \quad (2)$$

where  $\Delta W_{pot}$  is the difference between the potential energies of the streamer's tip and of the new sphere of positive ions built up by the new series of avalanches (namely, the new streamer tip),  $W_g$  the energy gain attributed to the applied field and  $W_l$  the total loss of energy during the formation of the new avalanches. The streamer continues to propagate if the starting point of the equivalent avalanche is located within the active region.

The streamer propagation model was completed by calculation of the current at each time step using the Ramo-Shockley theorem (Ramo 1939, Shockley 1938). The individual streamer filament has two current components: a positive ion component arising from the apparent movement of the positive streamer head with its propagation velocity and an electronic component arising from the movement of electrons in the streamer channel (Bondiou and Gallimberti 1994).

#### 3.3. Simulation results

For the reference experimental set-up, the calculation gave a threshold streamer inception voltage of 159 kV. To study the effect of the statistical time lag, 200, 300 and 400 kV were also used as representative values of the actual inception voltage.

The output data generated by the streamer propagation model include quantities such as the development with time of the position of the streamer's head and the head's radius, the number of positive ions in the streamer's head, the streamer's velocity and the current measured at the electrode. Typical results of the streamer propagation model are presented in figure 3 for a gap voltage of 159 kV. If the streamer propagation model is coupled with the circuit model (1) the effect of the series resistance of the circuit can be studied. With  $R = 1 \text{ M}\Omega$  ( $C_g = 6 \text{ pF}$  and  $C_R = 15 \text{ pF}$ ), no appreciable difference can be identified in the propagation characteristics plotted in figure 3. A quantitative study of the influence of the series resistor for various values of the actual streamer inception voltage is presented in table 1. It reveals that the influence of the series resistance on the extension and charge of the streamer is of the order of 0.1%.

**Table 1.** The influence of the series resistance on the streamer's propagation distance ( $x_s$ ) and the total charge at the electrode ( $q_s$ ), where  $U_{inc}$  is the streamer inception voltage.

$U_{inc}$ (kV)	$R = 0$		$R = 1 \text{ M}\Omega$		Difference	
	$x_s$ (mm)	$q_s$ (pC)	$x_s$ (mm)	$q_s$ (pC)	$\Delta x_s$	$\Delta q_s$
159	70.78	17.10	70.67	17.09	-0.1%	-0.1%
200	103.0	26.52	102.8	26.48	-0.2%	-0.2%
300	192.2	53.30	191.9	53.25	-0.2%	-0.1%
400	306.3	86.85	306.0	86.80	-0.1%	-0.1%

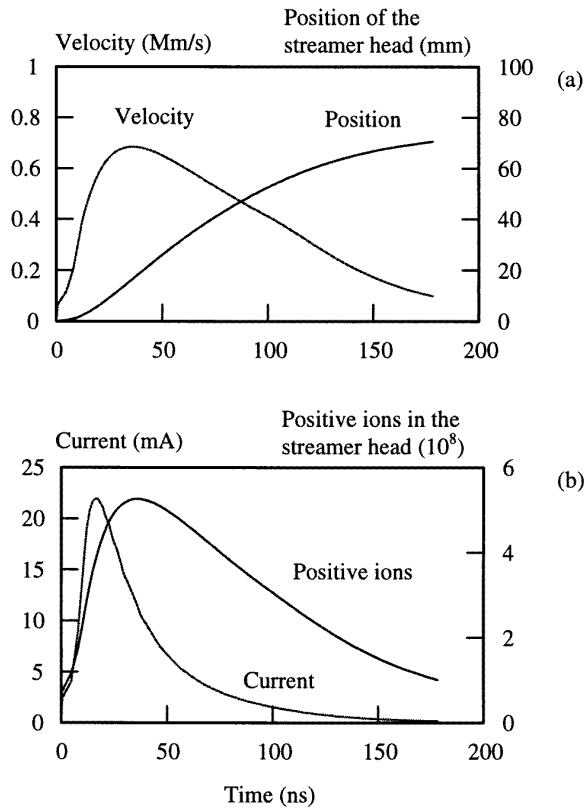


**Figure 3.** Typical results from the streamer propagation model, showing the propagation parameters of a streamer.

#### 4. The streamer–leader system phase

##### 4.1. The second streamer corona and leader inception model

The charge injected into the gap by the first corona produces a space-charge field that reduces the total electrical field strength in the vicinity of the electrode. Depending on the value of the radius of curvature of the high-voltage rod electrode, a dark period takes place (Les Renardières Group 1974, Gallimberti 1979). The subsequent phase of the discharge is the inception and development of the second corona; this phase also includes the inception of the leader channel. The dominant mechanism for the transition from streamer filaments to a leader channel is the heating of the filament by Joule heating and relaxation of the vibrational energy to the critical temperature. At this temperature,

around 1500 K, the thermal detachment of negative ions enhances the conductivity and lowers the internal field.

The second and successive streamer corona threshold inception voltages can be calculated by assuming that the space charge of the previous streamer corona reduces the electrical field strength at the electrode's tip to the streamer propagation stability field strength  $E_{stab}$  (Goelian *et al* 1997). Hence, the increase in applied voltage needed for inception of each successive streamer corona is given by

$$\Delta U_{inc} = U_{inc} - E_{stab}/E_N \quad (3)$$

where  $U_{inc}$  is the voltage for inception of the first streamer and  $E_N$  is the normalized Laplacian electrical field strength at the electrode's tip.  $E_N = E/U$ , the electrical field strength divided by the applied voltage.

##### 4.2. The streamer–leader propagation model

Once a leader is initiated, a streamer–leader system will propagate into the gap. The system is depicted in figure 4 and the main features are as follows (Bondiou and Gallimberti 1994). The streamer filaments in the leader corona form a diffuse glow discharge which converges at the leader's tip. The current collected by the leader's tip determines the energy used in the transition from a diffuse glow to a leader channel: the focusing of the current and field lines towards the leader's tip produces a strong enhancement of the power density input, which increases the local gas temperature to above the critical temperature for detachment of negative ions. The propagation of the leader's tip in the gap sustains the electrical field in the active corona front and, hence, supports the ionization phenomena necessary for propagation of the corona streamers. The system stops propagating when the electrical field in the active corona front becomes too low to support streamer propagation.

The development of a positive spark in *long* gaps (several metres) is characterized by the propagation of the streamer–leader system and plays only a minor role in 1 m gaps, for which the streamer corona bridges the gap quickly and launches the final jump (Meek and Craggs 1978). To investigate the influence of a large series resistance on the streamer–leader system, calculations have been performed for a 5 m gap, one in which the streamer–leader system clearly dominates. The analysis of the streamer–leader propagation follows the model presented by Goelian *et al* (1997).

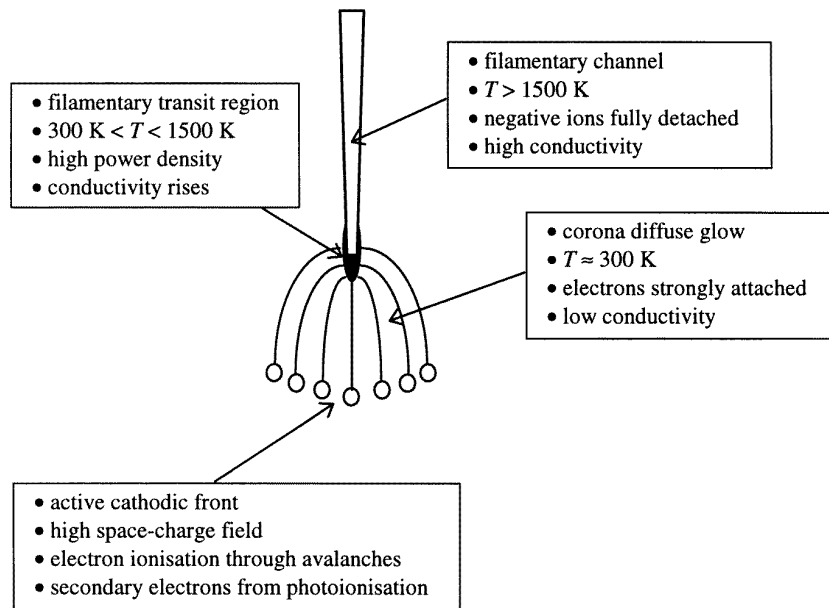


**Figure 4.** The physical structure in the front of a propagating leader discharge. Adapted from Bondiou and Gallimberti (1994).

### 4.3. Simulation results

The simulation was done for a 5 m rod-to-plane gap configuration in which the rod electrode had a hyperboloid-shaped tip with a radius of curvature of 5 mm. A 250/2500  $\mu\text{s}$  impulse voltage with a crest of 1.4 MV was used as the applied voltage. Typical results are presented in figure 5. Again, if the streamer propagation model is coupled with the circuit model (1), the effect of the series resistance of the circuit can be studied. The results of the simulation are presented in figure 6 for the circuit parameters  $R = 0.5 \text{ M}\Omega$ ,  $C_R = 15 \text{ pF}$  and  $C_g = 50 \text{ pF}$ . Figures 5(a) and 6(a) represent the propagation of the discharge as artificial streak photographs, such that the top of each figure represents the position of the rod electrode and the bottom represents the position of the plane electrode. The triangles in figures 5(a) and 6(a) represent the extension of the streamer corona. Figures 5 and 6 show that the series resistor limits the leader current and slows down the propagation of the streamer-leader system. Without a series resistance, the leader corona streamers bridged the electrode gap after 190  $\mu\text{s}$ , but, for  $R = 0.5 \text{ M}\Omega$ , the leader corona front stopped propagating after 255  $\mu\text{s}$ .

The calculated discharge characteristics are summarized in table 2. The delay in the corona inceptions and the absence of a change in the corona extensions are attributable to the voltage division, shown in figure 2(a). Since no statistical time lag is introduced, the calculations give the corona's extension at the threshold inception voltage. This means that the inception time is delayed, whilst the inception voltage remains unaffected. Table 3 shows that the disruptive discharge voltage and time-to-breakdown increase with the series resistance. It can thus be concluded from the simulations that the presence of a large series resistance in the discharge circuit does indeed slow down

**Table 2.** Calculated times and extensions for the 5 m rod-to-plane gap with and without an inhibiting series resistor for an applied crest voltage of 1.4 MV.

	Series resistance		
	0	0.5 M $\Omega$	1.0 M $\Omega$
First corona	4.5 $\mu\text{s}$	13 $\mu\text{s}$	16 $\mu\text{s}$
	0.11 m	0.11 m	0.11 m
Second corona	8.8 $\mu\text{s}$	22 $\mu\text{s}$	27 $\mu\text{s}$
	0.31 m	0.31 m	0.31 m
Leader channel	190 $\mu\text{s}$	255 $\mu\text{s}$	263 $\mu\text{s}$
	2.4 m	1.0 m	0.56 m
Leader corona	190 $\mu\text{s}$	255 $\mu\text{s}$	263 $\mu\text{s}$
	2.6 m	2.4 m	2.1 m

the propagation of streamer-leader systems and that it increases the disruptive discharge voltage.

## 5. The final jump phase

The final jump starts when the front of the leader corona reaches the plane and this is the terminal stage of the propagation of the streamer-leader system. It is characterized by an increase in the current and acceleration of the leader tip, which leads to short circuiting of the gap (Gallimberti 1979). A model of the final jump is presented in section 5.1, the simulation results are presented in section 5.2 and a comparison with the experimental data is made in section 5.3.

### 5.1. The final jump model

The final jump starts when the leader corona has bridged the gap. Three sets of equations have been established in order to calculate the propagation of the leader's tip during the final jump. The first set of equations is the

**Table 3.** Calculated values of the disruptive discharge voltage and time to breakdown as functions of the value of the series resistance.

	Series resistance				
	0	0.2 MΩ	0.5 MΩ	1 MΩ	2 MΩ
Critical voltage, $U_{50\%}$ (MV)	1.4	1.45	1.6	1.9	2.4
Time to breakdown ( $\mu$ s)	190	246	328	383	472

differential equation of the equivalent circuit (1), described in section 2, in which the gap voltage is calculated. The applied voltage  $U_0$  and the discharge current  $I_d$  are needed as input parameters. The second set of equations (general equations) calculates leader propagation parameters, such as the channel extension and current, as functions of time. The third set of equations (local equations) calculates the leader channel's characteristics as functions of time and position, examples of these characteristics being the local voltage gradient, the channel radius and the temperature. SI units are used in all equations.

**5.1.1. General equations.** The velocity of the leader's tip during the final jump across a 1 m rod-to-plane gap subjected to a lightning impulse voltage has been studied experimentally by Baldo and Pesavento (1983). They established the following interpolation formula for the leader's velocity  $v_l$ :

$$v_l = 0.3(E_{ss} - E_{stab}) + 0.1 \times 10^{-6} \frac{dU}{dt} \quad (4)$$

where  $E_{ss}$  is the mean electrical field strength across the gap between the leader's tip and the plane electrode,  $E_{stab}$  is the stability field for streamer propagation and  $U$  is the gap voltage.  $E_{ss}$  is given by

$$\begin{aligned} E_{ss} &= U_{lt}/(d - x_l) \\ U_{lt} &= U - \int_0^{x_l} E_l dx \\ x_l &= \int_0^t v_l dt' \end{aligned} \quad (5)$$

where  $U_{lt}$  is the potential of the leader's tip,  $x_l$  the leader's length and  $E_l$  the local voltage gradient in the leader channel. The second term of equation (4), which takes into account the rate of the rise in the applied voltage, is negligible for the present study because of the long time to crest (100  $\mu$ s).

The current injected into the leader channel ( $I_l$ ) can be expressed as the leader's velocity ( $v_l$ ) multiplied by the charge per unit length ( $q_l$ ):

$$I_l = v_l q_l. \quad (6)$$

On the basis of a thermodynamic model of the leader channel (Gallimberti 1979), the charge per unit length can be expressed in the form

$$q_l = \frac{50 \times 10^{-6} + 10^{-9} v_l (1 + v_l / 10^4)}{1 + 90 / (1 + 3.2 \times 10^{-3} v_l)}. \quad (7)$$

**5.1.2. Local equations.** The expansion of the leader's channel can be represented (Gallimberti 1979) by the following ordinary differential equation for a channel of cross section  $S$ :

$$\frac{\gamma p}{\gamma - 1} \frac{dS}{dt} = E_l I_l \quad (8)$$

where  $p$  is the pressure and  $\gamma$  the heat capacity ratio. Assuming that the number of neutral molecules within the channel remains constant during the expansion, the gas density is then given by

$$n = n_0 \frac{S_0}{S} \quad (9)$$

where  $n_0$  and  $S_0$  are the initial values of the gas density and the cross section of the channel, respectively. The initial gas density was set to  $4.89 \times 10^{24} \text{ m}^{-3}$  (corresponding to a gas temperature of 1500 K) and the initial channel radius was set to 300  $\mu$ m (Gibert and Bastien 1989, Aleksandrov *et al* 1995). The internal voltage gradient  $E_l$  was calculated for every channel segment, by using two different models, one for a cold channel (non-thermalized) and the other for a hot one (thermalized).

The model for the cold channel is based on the expansion of the leader channel by Joule heating, with a constant number of neutral gas molecules (Gallimberti 1979). In this case, the reduced electric field  $E/n$  assumes an almost constant value of  $E/n = 0.75 \times 10^{-19} \text{ V m}^2$  (Gallimberti 1979), giving

$$E_l = 0.75 \times 10^{-19} n. \quad (10)$$

The hot-channel model is based on the assumption that the current density in the thermalized channel is due to the drift of electrons produced by thermal ionization. One ends up with

$$E_l = \frac{I_l}{S} \frac{1}{e i n \mu_e} \quad (11)$$

where  $i$  is the degree of ionisation and  $\mu_e$  the electron mobility. The degree of ionization, derived from a detailed channel model (Bondiou 1991), is given by the following interpolation formula:

$$\log(i) = -14.220 + 2.1632 \times 10^{-3} T - 9.1691 \times 10^{-8} T^2 \quad (12)$$

in the temperature interval 4500–10000 K. The temperature  $T$  is calculated using the ideal gas law:

$$T = \frac{p}{n k_B}. \quad (13)$$

The transition temperature  $T_{th}$  relevant for the change-over between the cold- and the hot-channel models is assumed

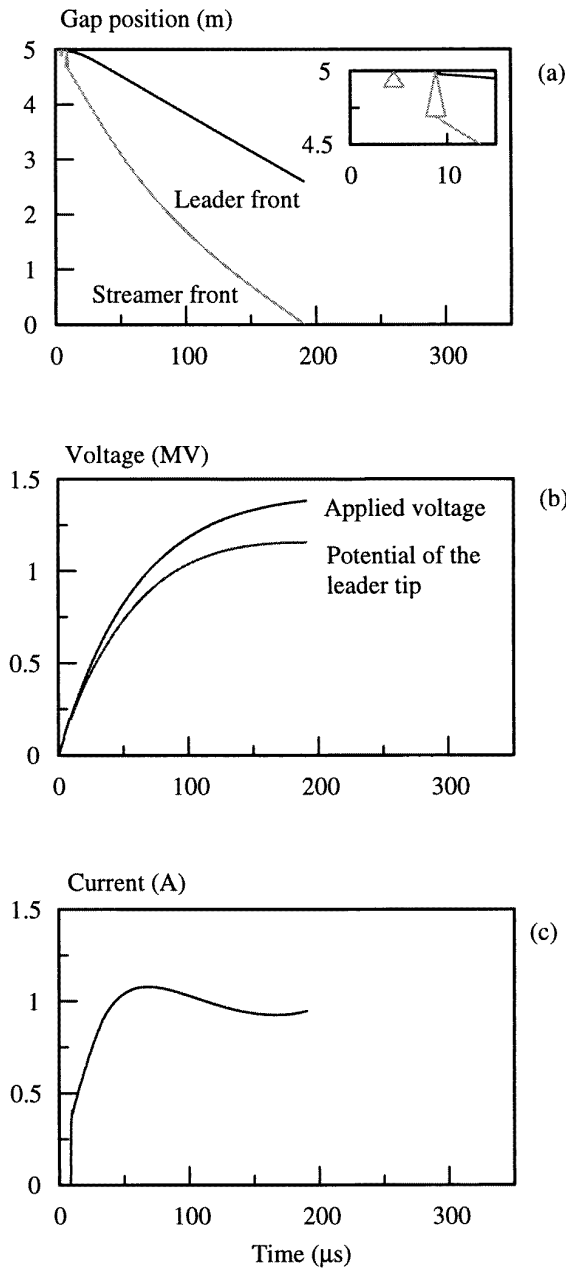


**Figure 5.** Propagation characteristics of the streamer-leader system for a 5 m rod-to-plane gap without an inhibiting series resistance. (a) An artificial streak photograph with an enlargement of the first 15  $\mu\text{s}$  in which the triangles represent the corona extension. (b) The applied voltage and the leader tip's potential. (c) The leader's current.

to occur with the thermalization, which is given by the following interpolation formula:

$$T_{ih} = 5202 + 648.9 \log(i). \quad (14)$$

## 5.2. Simulation results

Figure 7 gives a flow chart of the numerical simulation of inhibited discharges, taking into account the subsequent

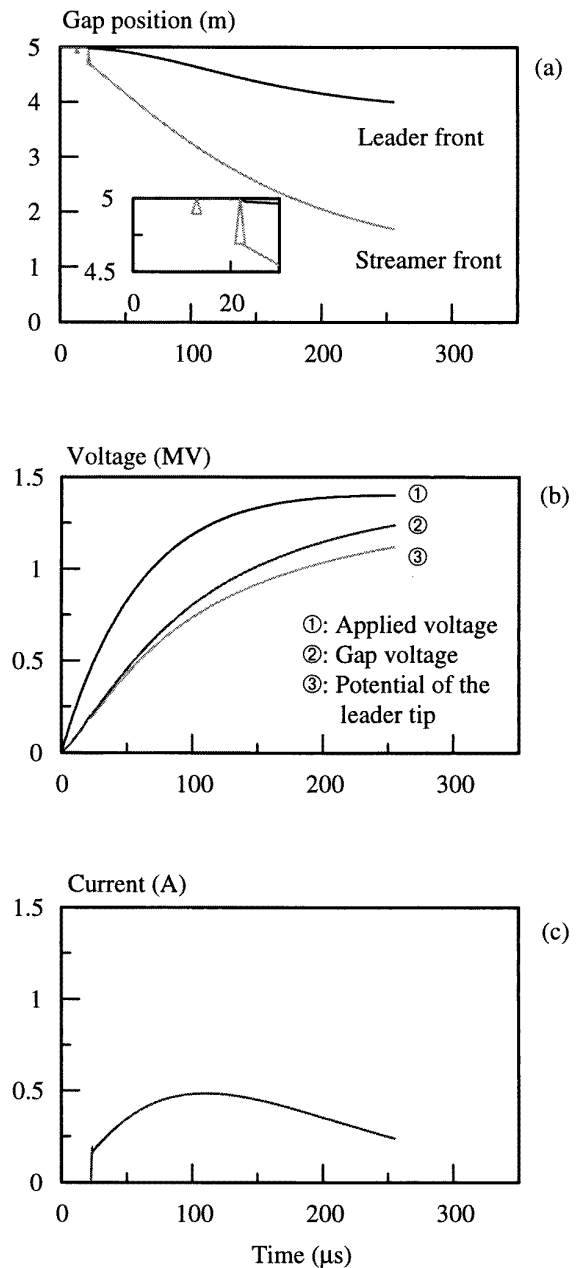


**Figure 6.** The same as figure 5, but with a 0.5  $\text{M}\Omega$  inhibiting series resistance. A comparison with figure 5 shows that the series resistance limits the discharge current and slows down the propagation.

phases of the spark formation. For the reference experimental set-up, the applied voltage was a 80/3000  $\mu\text{s}$  impulse with a crest voltage of 550 kV; the circuit parameters were  $R = 1 \text{ M}\Omega$ ,  $C_R = 15 \text{ pF}$  and  $C_g = 6 \text{ pF}$ . Under these conditions, the development of the streamer-leader phase is negligible since the streamer corona quickly bridges the gap.

The threshold streamer inception voltage was calculated to be 159 kV. The first corona occurs at  $t = 7 \mu\text{s}$  and has an extension of 0.21 m. The successive streamer inceptions occur at  $t = 17, 36$  and  $112 \mu\text{s}$ , with corona extensions of

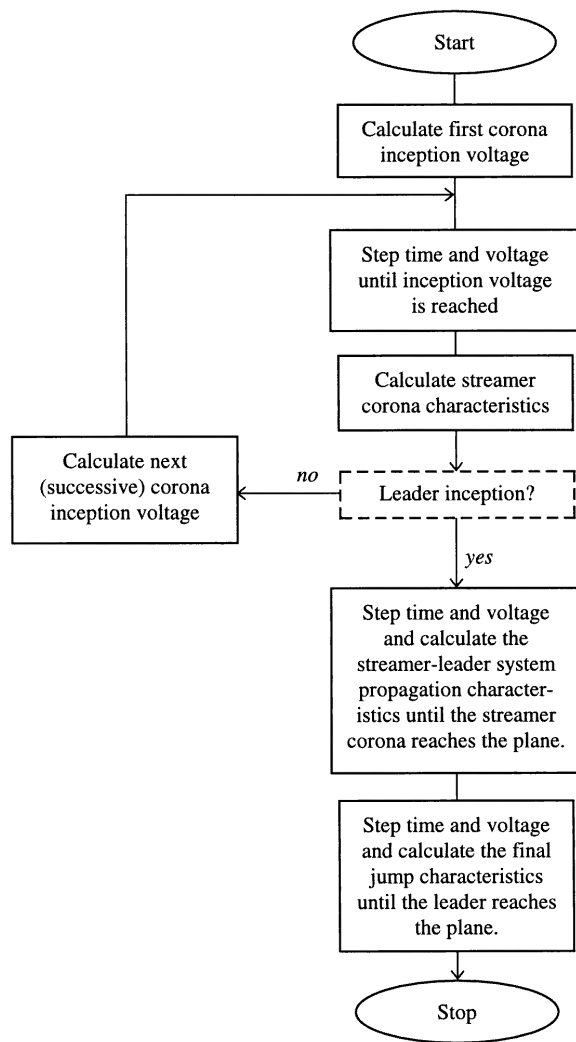


**Figure 7.** A flow chart of the inhibited discharge model.

0.5, 0.82 and 1 m, respectively. These data are shown in figure 8(a) in the form of an artificial streak photograph. The top and bottom of figure 8(a) represent the positions of the rod and plane electrodes, respectively. The corona current impulses are presented in figure 8(c); figure 8(b) shows the applied voltage and the gap voltage.

The fourth streamer corona bridges the gap and thus initiates the final jump. Figure 8(a) shows the propagation of the leader channel, which starts at 112  $\mu\text{s}$  and bridges the gap at 190  $\mu\text{s}$ . In figure 8(b), the potential of the leader tip is plotted in addition to the applied voltage and the gap voltage. Figure 9(a) shows the leader tip's velocity and figure 9(b) shows the mean voltage gradient of the leader channel. Figure 9(c) shows the fraction of the leader channel that has been thermalized during its propagation.

**5.3. Comparison between simulated and measured results**

In figure 10 the voltage and current oscillograms for a disruptive discharge are shown. A comparison between

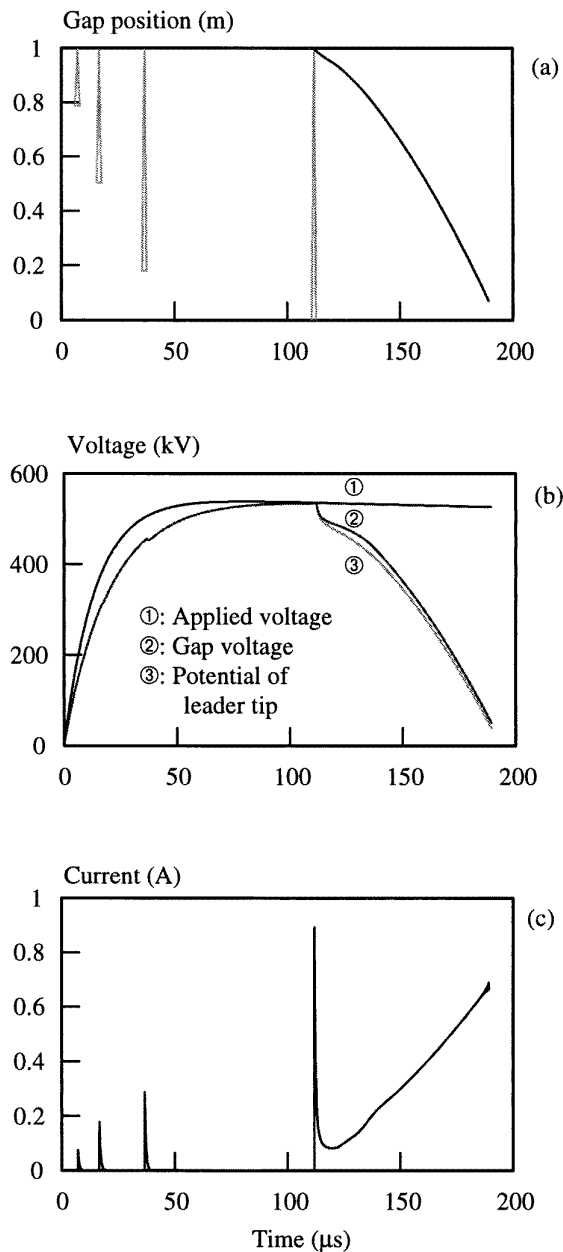


**Figure 8.** Simulated inhibited discharge characteristics. (a) An artificial streak photograph. (b) Voltage traces. (c) The discharge current (at the rod electrode).

figure 10 and figures 8(b) and (c) demonstrates how appropriate the model is. The first and second corona current impulses are clearly visible, as predicted by the simulation, in the measured oscillogram. The fourth corona, that which bridges the gap and initiates the final jump, occurs later than predicted by the simulation. However, there was significant scatter in the time measured to the initiation of the final jump ( $155 \pm 53 \mu\text{s}$ ) and the theoretical value (112  $\mu\text{s}$ ) falls well within this. The deviation between the predicted and measured corona current amplitudes may be attributed to the simple streamer model, which neglects the streamer's structure

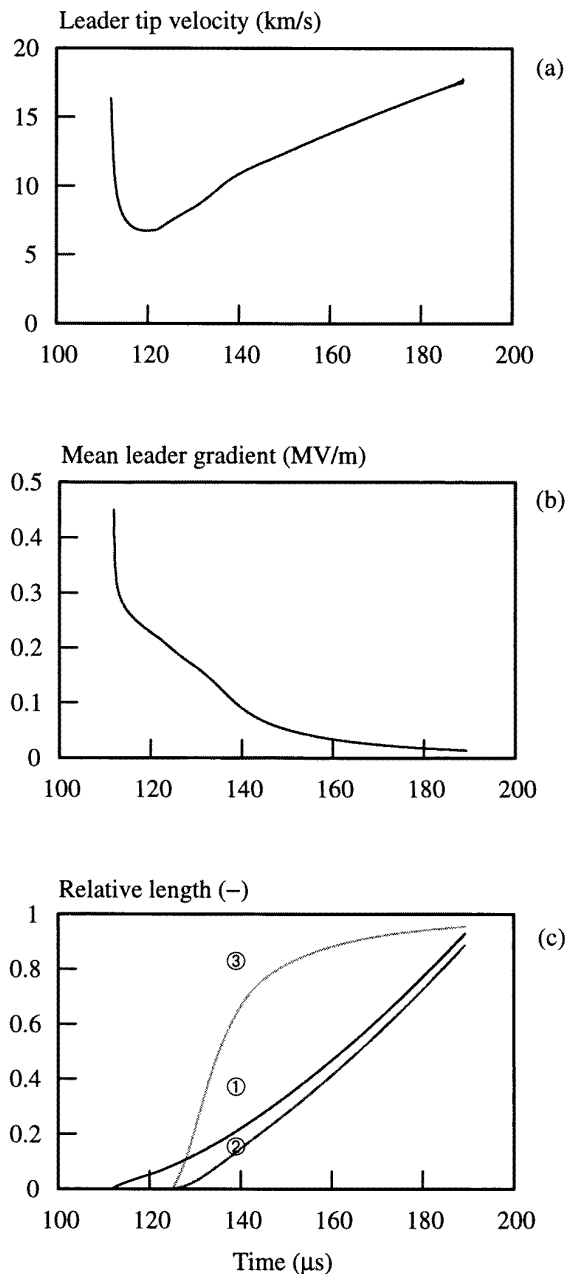


**Figure 9.** More simulated inhibited discharge characteristics. (a) The velocity of the leader's tip. (b) The mean leader channel voltage gradient. (c) Plots of 1, the fraction of the gap covered by the leader channel; 2, the fraction of the gap covered by the thermalized channel; and 3, the ratio of the length of the thermalized channel to the total length of the leader channel.

and branching, and to the limited resolution of the current measurement.

The predicted behaviour of the voltage and current during the final jump agrees well with the measured results. The current of the corona crossing the gap gives a small, but fast, reduction in the gap voltage; as the leader channel propagates in the gap, the gap voltage decreases and the current slowly increases. The duration of the final jump ( $78 \mu\text{s}$ ) is a little longer than the measured value ( $55 \pm 7 \mu\text{s}$ ). Furthermore, the leader current is about a factor

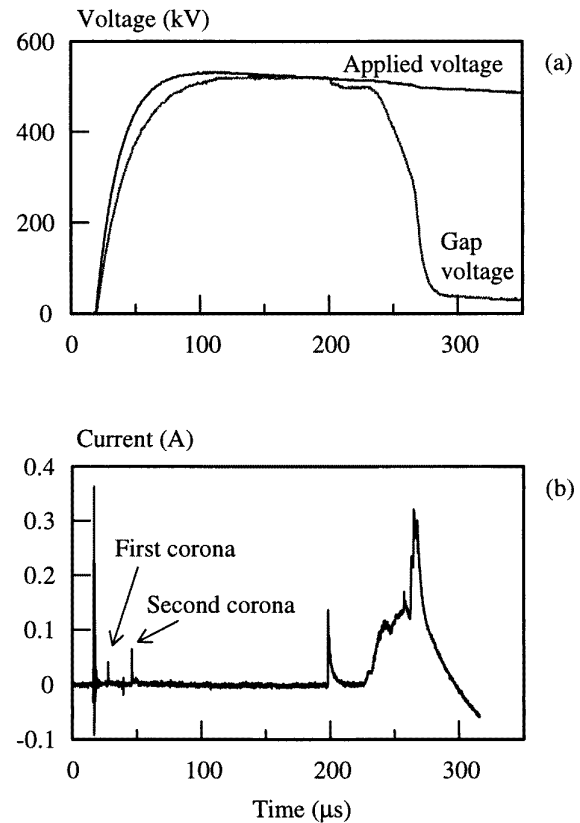


**Figure 10.** Measured inhibited discharge characteristics. (a) Voltage oscillograms. (b) The discharge current (at the rod electrode). A comparison with figures 8(b) and (c) reveals satisfying agreement between simulations and measurements.

of two higher than the measured value. However, taking into account the fact that simplified models and empirical relationships have been used, the agreement between the calculations and the measured data is satisfying.

## 6. Conclusions

The most important consideration in modelling an inhibited discharge is to account properly for the influence of the external circuit in which the discharge current flows. For the 1 m discharge gap, the simple circuit shown in figure 1(b) is an adequate equivalent circuit for inhibited discharge simulations. The capacitance and resistance of the circuit can easily be measured or calculated. In order to calculate the discharge current, physical models of the streamer corona, the streamer-leader system and the final jump have been implemented. The main results of the calculations were

- (i) streamer propagation is *not* inhibited by a large series resistance,
- (ii) propagation of the streamer-leader system is inhibited by a large series resistance and
- (iii) the final jump *is* inhibited by a large series resistance.

The experimental results presented by Larsson (1998) have confirmed conclusions (i) and (iii).

### Acknowledgments

The authors would like to thank Professor Viktor Scuka for his continuous interest in and support of this work. The support of Dr Philippe Lalande and the rest of the staff at the Discharge Modelling Group at ONERA is deeply appreciated. One of the authors (AL) acknowledges financial support from the Swedish Transmission Research Institute (STRI).

### References

Ace 1996 ABB common platform for field analysis and simulation – user manual, ABB Corporate Research Internal Report (Västerås)  
Aleksandrov N L, Bazelyan A E, Bazelyan E M and Kochetov I V 1995 *Plasma Phys. Rep.* **21** 57

Baldo G and Pesavento G 1983 *Proc. 4th Int. Symp. on High-Voltage Engineering (Athens)*  
Bondiou A 1991 ONERA report DRET No 99/7154PY  
Bondiou A and Gallimberti I 1994 *J. Phys. D: Appl. Phys.* **27** 1252  
Gallimberti I 1972 *J. Phys. D: Appl. Phys.* **5** 2179  
———1979 *J. Physique Coll.* **40** C7-193  
Gibert A and Bastien F 1989 *J. Phys. D: Appl. Phys.* **22** 1078  
Goelian N, Lalande P, Bondiou-Clergerie A, Bacchiega GL, Gazzani A and Gallimberti I 1997 *J. Phys. D: Appl. Phys.* **30** 2441  
Larsson A 1997 *Inhibited Electrical Discharges in Air* (Stockholm: Almqvist & Wiksell International)  
———1998 An experimental study of inhibited electrical discharges in air *J. Phys. D: Appl. Phys.* **31** 1823  
Larsson A and Scuka V 1997 *Proc. 10th Int. Symp. on High-Voltage Engineering (Montréal)*  
Les Renardières Group 1974 *Electra* **35** 49  
Meek J M and Craggs J D (eds) 1978 *Electrical Breakdown of Gases* (Chichester: Wiley)  
Ramo S 1939 *Proc. IRE* **27** 584  
Shockley W 1938 *J. Appl. Phys.* **9** 635